COMPUTED TOMOGRAPHY OF TRANSVERSE PHASE SPACE*

A. Watts†, C. Johnstone‡, J. Johnstone§
Fermilab, Batavia, IL, USA

Abstract

Two computed tomography techniques are explored to reconstruct beam transverse phase space using both simulated beam and multi-wire profile data in the Fermilab Muon Test Area ("MTA") beamline. Both Filtered Back-Projection ("FBP") and Simultaneous Algebraic Reconstruction Technique ("SART") algorithms [1] are considered and compared. Errors and artifacts are compared as a function of each algorithm's free parameters, and it is shown through simulation and MTA beamline profiles that SART is advantageous for reconstructions with limited profile data.

BEAM PROJECTION

Computed tomography reconstructs an N-dimensional object out of many (N-1)-dimensional projections, examples of which are pictured in Fig. 1. Similarly, a transverse beam profile is a one-dimensional projection of the two-dimensional phase space. Computed tomography is thus the reverse of the projection process, i.e. integrating many (N-1)-dimensional projections into a reconstructed N-dimensional image. For a full reconstruction, profile data must exist through a viewing angle range of π radians [1]. However, to use any computed

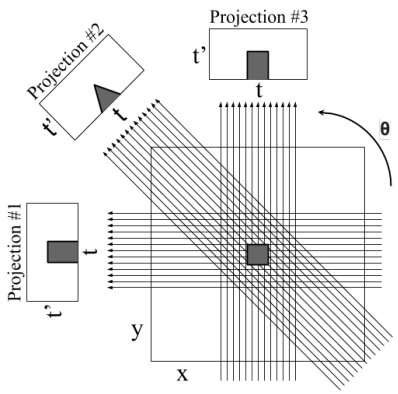

Figure 1: 1-D projection of a 2-D object. Traditional tomography is the reverse of the projection process.

tomography algorithm, an analogy must be made between such projections of a physical object and beam profiles [2]. For the projection in Fig. 1, the coordinate systems of the image and a projection are related by:

$$\begin{pmatrix} t \\ t' \end{pmatrix} = \begin{pmatrix} cos\theta & sin\theta \\ -sin\theta & cos\theta \end{pmatrix} \begin{pmatrix} x \\ x' \end{pmatrix} \quad (1)$$

So the projection onto the t axis of a ray passing through pixel (x, x') of the original image at angle θ is:

$$t = xcos\theta + x'sin\theta \quad (2)$$

Thus Equation 3 describes the general projection $P(t, \theta)$ onto axis t at viewing angle θ of two-dimensional object $f(x, y)$.

$$P(t, \theta) = \iint dxdy f(x, y)\delta(xcos\theta + ysin\theta - t) \quad (3)$$

Similarly, neglecting dispersion, the phase space coordinates for a particle at two locations in a beamline with only linear forces are related by:

$$\begin{pmatrix} x_2 \\ x_2' \end{pmatrix} = \begin{pmatrix} R_{11} & R_{12} \\ R_{21} & R_{22} \end{pmatrix} \begin{pmatrix} x \\ x' \end{pmatrix} \quad (4)$$

By defining the phase orientation angle $\theta = tan^{-1}(\frac{R_{12}}{R_{11}})$ and scaling factor $s = \sqrt{R_{11}^2 + R_{12}^2}$, such that $R_{11} = scos\theta$ and $R_{12} = ssin\theta$ the beam projection can be rewritten as:

$$P(x_2, \theta) = \iint dxdx' f(x, x')\delta(s[xcos\theta + x'sin\theta - \frac{x_2}{s}) \quad (5)$$

For beam, each projection $P(x_2, \theta)$ is a profile measured with instrumentation like a multi-wire detector. Thus computed tomography algorithms may be used to reconstruct beam transverse phase space if each profile is scaled horizontally by $\frac{1}{s}$ and vertically by s, and if the appropriate scaling factor and phase orientation angle for each profile are known. Whereas traditional tomography involves rotating a camera around a fixed object, beam tomography rotates the phase space distribution while taking projections (i.e. beam profiles) at the same location in the beamline.

BEAM SIMULATION

To test the efficacy of the computed tomography algorithms, a simple linear particle tracking Python code was used to build profile data while varying the phase orientation angle of a simple FODO channel beamline. A deliberately non-elliptical and asymmetric beam distribution was generated particle-by-particle, each of which being passed through the beamline using the thick-lens linear transfer matrix.

A multiwire profile monitor was simulated by taking a histogram of all particle 'x' values with 48 bins spaced 1 mm apart; this is typical for the number of wires and spacing for Fermilab SEM multiwires. For every quadrupole value in the scan of phase rotation angle ranging π radians, a histogram profile is taken at the end of the beamline. The initial beam distribution is pictured in Fig. 2 in two-dimensional histogram form. Reconstruction of this simulated data at the beginning of the beamline was carried out using the "scikit-image" Python library [3].

* Work supported by Fermi Reserach Alliance, LLC under Contract no. DE-AC02-07CH11359 with the United States Department of Energy.
† awatts@fnal.gov
‡ cjj@fnal.gov
§ jjohnstone@fnal.gov

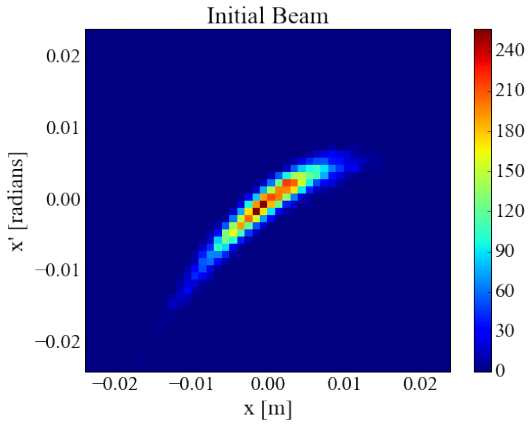

Figure 2: Simulated initial beam distribution in 48x48 bin 2-D histogram to mimic multi-wire resolution. The color scale represents the number of particles in a given pixel.

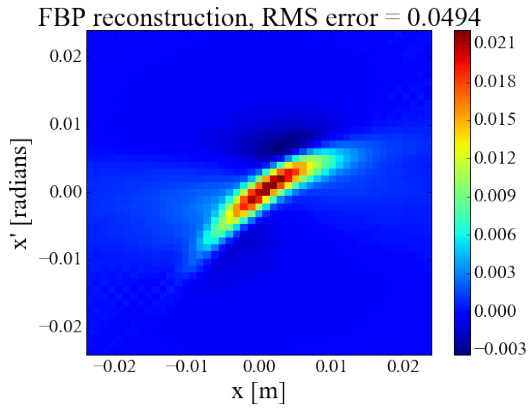

Figure 3: Filtered Back Projection reconstruction. The color scale is normalized so the sum of all pixels is unity.

FILTERED BACK PROJECTION

Filtered Back Projection ("FBP") is a common computed tomography method first applied to transverse phase space reconstruction by McKee *et. al.* in 1995 [4]. This method applies a standard filter to each projection before "back-projecting" each and allowing them to interfere; the interference pattern forms the reconstructed image.

Described by Eq. (6), the FBP reconstruction process involves computing the Fourier Transform $R(\omega, \theta)$ of each profile $P(t, \theta)$, then simultaneously back-projecting through $t = xcos(\theta) + ysin(\theta)$ and computing the inverse Fourier Transform. Finally, integrating over all projection angles produces the reconstruction.

$$f(x, y) = \iint \omega d\omega d\theta e^{2\pi i(\omega x cos\theta + \omega y sin\theta)} F(\omega) R(\omega, \theta) \tag{6}$$

The filter $F(\omega)$ is one of the free parameters for FBP reconstruction. Comparing the RMS errors for reconstruction using each available filter in the Python library, it was determined that the "ramp" filter $F(\omega) = |\omega|$ provided the best reconstruction. Each pixel of both the original histogram and the reconstruction are normalized by the sum of all pixel values, so the sum of all pixels for each image is unity. The error for each pixel is computed by subtracting the reconstruction pixels from the original histogram pixels. Finally, the total RMS error is computed for the entire error image. This allows for a quantitative comparison between tomography methods. The FBP reconstruction and associated RMS error are shown in Fig. 3.

SIMULTANEOUS ALGEBRAIC RECONSTRUCTION TECHNIQUE

Simultaneous Algebraic Reconstruction Technique ("SART") takes a different approach to tomography than FBP by considering a ray of finite thickness intercepting the image to be reconstructed. This is shown in Fig. 4, where each projection at angle θ is the sum of rays p_i, and f_j is

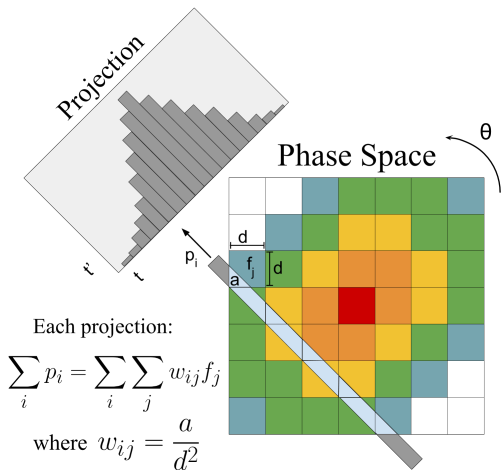

Figure 4: Diagram of a ray intercepting a pixellated image for the purpose of SART reconstruction.

value of the "j" pixel. Each ray intercepts a fractional area of a pixel $w_{ij} = \frac{a_{ij}}{d^2}$. Therefore, the original image may be reconstructed from projections by solving linear system in Eq. (7) that shows how each "bin" of a projection is determined from the "i" ray interacting with the "j" pixel for N total pixels [1].

$$\sum_{j=1}^{N} w_{ij} f_j = p_i \tag{7}$$

Thus w_{ij} is an M by N matrix, where M is the total number of all imaging rays for all projections, and N is the number of pixels in the image. Inversion of w_{ij} to solve for the value of each image pixel f_j would sufficiently reconstruct the original image; however, M and N are often very large, and often w_{ij} is not square, and thus cannot be directly inverted. However, w_{ij} is often sparse, because many pixels in an image may be blank, so only some pixels are intercepted by the imaging rays. Thus SART is an iterative method for solving Eq. (7) based on an algorithm originally developed by Stefan Kaczmarz and later developed by Kunio Tanabe known as the "method of projections" [5, 6]. The resulting reconstruction of the simulated data from Fig. 2 is pictured in

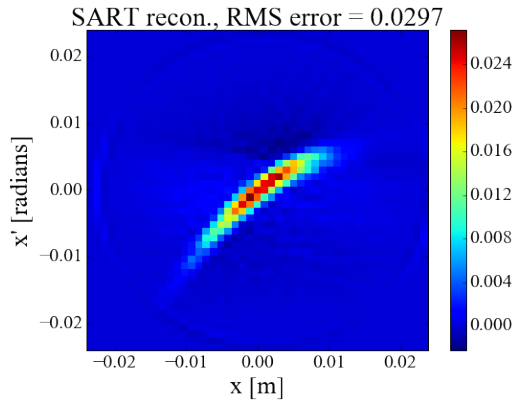

Figure 5: SART reconstruction. The color scale is normalized so the sum of all pixels is unity.

Fig. 5. The RMS error for SART is significantly lower than FBP, and beam tail reconstruction also appears improved.

Two main free parameters exist in the "scikit-image" Python library implementation of SART, namely the number of iterations and the "relaxation" value. A reconstruction from the first iteration of SART (i.e. the output of the "iradon-sart" function) is passed back into the function as an initial "guess". Successive iteration improves the RMS error, but eventually artifacts appear and propagate, so there is a maximum iteration number to achieve the best reconstruction. The relaxation value is the weighting factor $\alpha < 1$ on each pixel value as it is updated after each iteration. Thus a balance between relaxation and iteration number is necessary to provide the best reconstruction with minimal convergence time. Figure 6 shows how the RMS error of a SART reconstruction depends on both the iteration and the relaxation parameter. This plot informed the decision to use $\alpha = 0.1$ and 3 iterations for the reconstruction in Fig. 5.

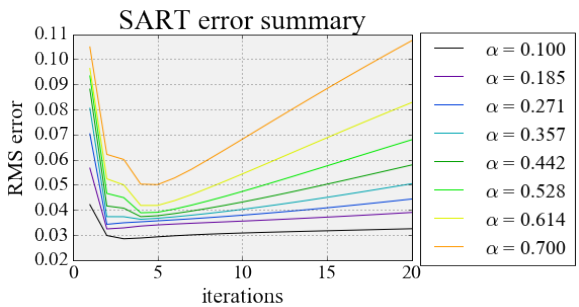

Figure 6: SART Reconstruction RMS error as a function of iteration and relaxation parameter.

MTA BEAM RECONSTRUCTION

To test the assertion [7] that the Fermilab MTA beam is non-elliptical in the vertical plane, a reconstruction of the vertical phase space was carried out using previously-acquired multiwire profile data. Pictured in Fig. 7, the reconstruction is limited by the low number of profiles that span a limited phase rotation angle range. The data is too limited to make a strong conclusion about the beam ellipticality, and a more detailed quadrupole scan should be considered in the future.

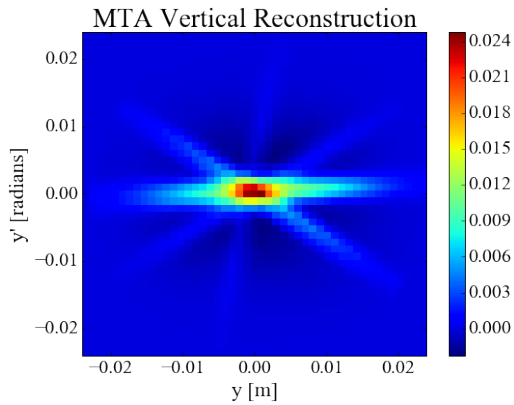

Figure 7: SART Reconstruction of MTA beamline vertical phase space. The color scale is normalized so the sum of all pixels is unity.

CONCLUSION

Both FBP and SART computed tomography algorithms have been compared to reconstruct the transverse phase space of a simulated beam. Error images were created with a pixel-by-pixel comparison of a 2-D histogram of the original distribution and each reconstruction, then an RMS error for each error image was computed. Using the RMS error as a figure-of-merit, it has been determined that the SART algorithm provides superior accuracy in reconstruction of a non-elliptical beam distribution. Further work will use such reconstructions to improve the optics match of transfer beamlines at Fermilab with non-elliptical beam from resonant extraction.

ACKNOWLEDGEMENTS

Diktys Stratakis, Phil Adamson, Ming-Jen Yang.

REFERENCES

[1] A.C. Kak and Malcolm Slaney, *Principles of Computerized Tomographic Imaging*, IEEE Press, 1988.

[2] J. Johnstone, "Phase Space Tomography with Dispersion," Fermilab Accelerator Division Beams Document #Beams-doc-5197-v1.

[3] Scikit-image website: `http://scikit-image.org/`

[4] C. B. McKee, P. G. O'Shea, J. M. J. Madey, "Phase Space Tomography of Relativistic Beams," *Nucl. Instrum. Methods Phys. Res.* A 358, 264 (1995).

[5] K. Tanabe, "Projection method for solving a singular system," *Numer. Math.*, vol. 17, pp. 203-214, 1971.

[6] S. Kaczmarz, "Angenäherte Auflösung von Systemen linearer Gleichungen," *Bull. Acad. Pol. Sci. Lett.* A, vol. 6-8A, pp. 355-357, 1937.

[7] A. Casacchia, "Investigation of Emittance Analysis Methods Using the Mucool Test Area," Fermilab SIST 2016.